Real-Time Experimental Demonstration and Evaluation of Open-Air Sense-and-Notch Radar

Jonathan Owen[1], Charles Mohr[1], Brandon Ravenscroft[1], Shannon Blunt[1], Benjamin Kirk[2], Anthony Martone[2]
[1] Radar Systems Lab (RSL), University of Kansas, Lawrence, KS
[2] Sensors and Electron Devices Division, Army Research Laboratory (ARL), Adelphi, MD

Abstract—**Recent work demonstrated closed-loop results for a real-time cognitive sense-and-notch radar capability via software-defined radio (SDR). The subsequent software-defined radar (SDRadar) generates spectrally shaped random FM (RFM) waveforms on-the-fly containing transmit spectral notches according to fast frequency assessments of other users in the band.**

Here we demonstrate the final cognitive evaluation step in which the sense-and-notch SDRadar operates in real-time in an open-air setting, performing moving target indication (MTI) processing (except for clutter cancellation) in the presence of a dynamically hopping interferer. This implementation is shown to support pulse repetition frequencies (PRFs) up to 4.4 kHz, meaning new interference-responsive waveforms can be produced at that rate, while achieving a transmit notch depth of 25 dB relative to peak power (greater depth is possible with additional computational resources).

Keywords—cognitive radar, real-time implementation, waveform agility, spectrum sharing

I. Introduction

Growing spectral congestion driven largely by proliferation of modern digital communications has created a number of challenges for radar [1-3], particularly given the need for improved sensitivity and discrimination despite the erosion of resources. Since this ravenous appetite for spectrum is a consequence of consumer cellular demand, which has a strong linkage to economic prosperity, it is possible that radars will be required to share spectrum with communications on a "not-to-interfere" basis at various times/places [3, 4].

In some respects, this condition is not new, since over-the-horizon (OTH) [5] and foliage penetration (FOPEN) [6] radars have for some time operated at frequencies where other primary users reside in order to make use of advantageous propagation effects. A wide variety of spectrally notched waveforms have also been developed (e.g. [7-12]). The rise of dynamic spectrum access (DSA) and agile transceivers, combined with the desire for greater radar bandwidth, is expected to expand the occurrence of this manner of operational footing in which radar seeks to maximize sensing functionality while also minimizing the mutual RF interference (RFI) it causes and receives.

This paper represents the culmination of a multi-year effort to achieve a real-time sense-and-notch radar capability that can contend with highly dynamic spectrum users. It consequently involves the intersection of practical waveform design, a novel method for efficient spectral notch generation, RF systems engineering for physical deployment, field-programmable gate array (FPGA) implementation for real-time processing, and assessment of a performance vs. computation trade-space.

Specifically, the FPGA of an Ettus x310 SDR was used to implement this SDRadar capability, consisting of the fast spectrum sensing (FSS) [13] algorithm to quickly assess the portions of the band occupied by other users on a per-pulse basis, followed by incorporation of corresponding spectral notches within a nonrepeating RFM waveform and the subsequent open-air transmission. Aspects of this approach were previously assessed in [14] using open-air measurements, though notched waveform generation was not yet real-time, and in [15] at real-time speeds, though not yet in an open-air setting. Here these attributes are combined to realize full sense-and-notch functionality in real-time for an MTI application.

II. Cognitive Spectral Notching via SDRadar

Nonrepeating RFM waveforms [16] provide inherent design freedom and flexibility that make them readily amenable to the incorporation of dynamic spectrum notching that can change (perhaps multiple times) during the radar coherent processing interval (CPI). Moreover, their FM structure is compatible with high-power transmitters due to constant amplitude and continuous phase attributes. The precision enabled by digital-to-analog converters (DACs) having significant bit-depth, in combination with such waveforms, then facilitates physical implementation of transmit spectral notching, though consideration of overall hardware distortion is still necessary [14, 17, 18].

For example, the analytical spectrum notching (ASpeN) method [19] involved development of an analytical model for the spectrum of a parameterized FM waveform to achieve notch depths better than 50 dB when using high-fidelity test equipment, which in [19] was a Tektronix AWG70002A arbitrary waveform generator (AWG). Yet subsequent generation of the same signal using a commercial off-the-shelf (COTS) SDR transceiver realized significant degradation of notch depth, necessitating reformulation of the waveform structural model to account for more modest SDR fidelity, particularly the far lower DAC rate and associated effects [17]. The resulting zero-order reconstruction optimization of waveforms (ZOROW) approach established a trade-space between notch depth and computational cost due to its recursive nature, though the ZOROW gradient-descent procedure permits the use of fast Fourier transforms (FFTs), which is vital for real-time implementation.

The stages within this sense-and-notch method are outlined in Table I, which also includes the latency of each stage when implemented on the FPGA of the SDR. The first stage is clearly the spectrum sensing process, which uses the FSS algorithm from [13] that was inspired by the human thalamus to quickly

This work was supported by the Army Research Office under Grant #W911NF-20-2-0271. DISTRIBUTION STATEMENT A. Approved for Public Release.

identify and aggregate a "good enough" partitioning of the operating band into appropriately sized subbands, which either do or do not contain a meaningful amount of RFI. The spectral locations and widths of the RFI-occupied subbands, collected in Ω, then inform where spectral notching is necessary.

Table I. Sense-and-notch stages with latencies

Algorithm	Latency
Fast Spectral Sensing (FSS)	120 μs
Pseudo-Random Optimized FM (PRO-FM)	28 μs / iteration
Zero-Order Reconstruction Optimization of Waveforms (ZOROW)	28 μs / iteration

Notched waveform generation then involves two sequential design stages. The first employs an efficient spectrally-shaped RFM design procedure, here chosen to be pseudo-random optimized (PRO) FM [20] because it relies on an alternating projection approach that is computationally efficient via the use of FFTs and simple projections. PRO-FM produces transmitter-suitable waveforms possessing a Gaussian power spectrum shape that realizes minimal sidelobes, though the incorporation of spectral notching realizes some degradation in that regard [14], requiring subsequent receive compensation when clutter cancellation is performed (e.g. [21-24]).

Let T be the pulse width, B the 3-dB bandwidth, and f_s the DAC rate, which for modest fidelity SDRs is not significantly greater than B (i.e. $f_s/B > 1$, but not $\gg 1$). Denote $\bar{\mathbf{s}}_q$ as the length-N digital representation of the desired analog waveform $\mathbf{s}_q(t)$ that the SDR intends to transmit for the qth of Q pulses in the CPI. Moreover, denote $\bar{\mathbf{s}}_q^{(k)}$ as the version of this vector after k iterations of PRO-FM alternating projections [20]

$$\bar{\mathbf{r}}_q^{(k+1)} = \mathbb{F}^{-1}\left\{\bar{\mathbf{g}} \odot \exp\left(j\angle \mathbb{F}\left\{\bar{\mathbf{s}}_q^{(k)}\right\}\right)\right\} \tag{1}$$

and

$$\bar{\mathbf{s}}_q^{(k+1)} = \bar{\mathbf{u}} \odot \exp\left(j\angle \bar{\mathbf{r}}_q^{(k+1)}\right), \tag{2}$$

where $\bar{\mathbf{s}}_q^{(0)}$ is a random initialization (constant amplitude and uniformly distributed in phase). Here $\mathbb{F}$ and $\mathbb{F}^{-1}$ are the Fourier and inverse Fourier transforms, respectively, $\angle(\bullet)$ extracts the phase of the argument, and $\odot$ is the Hadamard product. The length-N vector $\bar{\mathbf{g}}$ is a discretization of the magnitude spectral template $|G(f)|$, while length-N vector $\bar{\mathbf{u}}$ is a discretization of rectangular window $u(t)$ of duration T. Relative to the baseline notch-free form, the spectrum template in this context is modified for each sense-and-notch interval via

$$|G(f)| = 0 \text{ for } f \in \Omega. \tag{3}$$

This first stage of the notched waveform generation process provides the overall spectrum shaping and introduces the start of each spectrum notch, which has been found to facilitate rapid and efficient convergence overall. Because the PRO-FM approach can only achieve relatively shallow spectral notches, however, the ZOROW method is then applied to improve notch depth, while necessarily accounting for the modest f_s/B ratio of the DAC (in [17] the Tektronix AWG employed a ratio 50× greater than the Ettus x310 SDR).

Denoting the terminal $k = K$ iteration of PRO-FM as

$$\mathbf{s}_q = \exp(j\boldsymbol{\phi}_q), \tag{4}$$

where

$$\boldsymbol{\phi}_q = [\,\phi_{q,1}\;\; \phi_{q,2}\;\; \cdots\;\; \phi_{q,N}\,]^T, \tag{5}$$

ZOROW deepens the spectral notches while conforming to SDR hardware characteristics, in which each DAC input sample is held constant for $T_s = 1/f_s$ seconds. The resulting analog signal is then fed through a reconstruction filter to suppress repeated images outside the fundamental frequency interval of $[-f_s/2, +f_s/2]$.

It was shown in [19] that perfect Nyquist reconstruction can be analytically realized for a pulsed signal given sufficient sampling of the analytical spectrum. For the subsequent ZOROW representation [17], this sampled analytical spectrum has the form

$$\begin{aligned} S_q(f_m, \boldsymbol{\phi}_q) = {} & \frac{\sin(\pi f_m T_s)}{\pi f_m} \\ & \times \sum_{n=1}^{N} \exp\left(-j(2\pi f_m (n-1/2)T_s + \phi_{q,n})\right), \end{aligned} \tag{6}$$

where frequency $f_m = m\Delta f$ for integer m lies on the interval $-\infty < m < \infty$, as long as $f_m \le 1/(2T)$. Noting that (6) takes the form of a discrete Fourier transform (DFT) with an imposed sinc(·) envelope, it can be calculated efficiently using FFTs.

The ZOROW method then applies the cost function

$$J = \sum_m |\, S_q(f_m; \boldsymbol{\phi}_q)\,|^2, \tag{7}$$

where the indices in the summation correspond to the notch frequency interval(s) from (3). The gradient of (7) with respect to $\boldsymbol{\phi}_q$ is [17]

$$\mathbf{g}_q^{(\ell)} = 2\Im\left\{\tilde{\mathbf{A}}^H(\tilde{\mathbf{s}}_{\mathrm{f},q}^{(\ell)} \odot \tilde{\mathbf{w}}) \odot \mathbf{s}_q^{*(\ell)}\right\}, \tag{8}$$

which is implemented via gradient-descent to drive (7) toward zero. Here $\Im(\cdot)$ extracts the imaginary part of the argument, $\tilde{\mathbf{A}}^H$ is the $(2N-1)\times N$ truncated inverse DFT matrix, $(\cdot)^*$ is complex conjugation, $\mathbf{s}_q^{(\ell)}$ is (4) at the ℓth iteration of ZOROW, $\tilde{\mathbf{s}}_{\mathrm{f},q}{}^{(\ell)}$ is the Fourier transform thereof after padding with $N-1$ zeros, and the length $2N-1$ vector $\tilde{\mathbf{w}}$ captures the sinc(·) envelope in (6), where the frequencies associated with (7) are replaced by zeros. For example, the average spectral envelope of a given frequency-notched waveform optimized with $K = 2$ iterations of PRO-FM and $L = 6$ iterations of ZOROW, as used for the Ettus x310, is illustrated in Figure 1.

III. Implementation Considerations

A block diagram of the SDRadar cognitive radar architecture is shown in Fig. 2. The RF environment is sensed at the receive port of the SDRadar, where the signal is frequency down-converted and quantized into in-phase & quadrature channels at 100 MSamples/s, processed by a high-throughput FFT performed on the FPGA, and then continuously streamed to the host computer. Relative to [15], in which the latency of FSS on the host PC was $T_{FSS} = 3.1$ ms and therefore

served as the bottleneck in RFI identification, it has now been integrated onto the FPGA to operate in 120 μs, a 25× reduction.

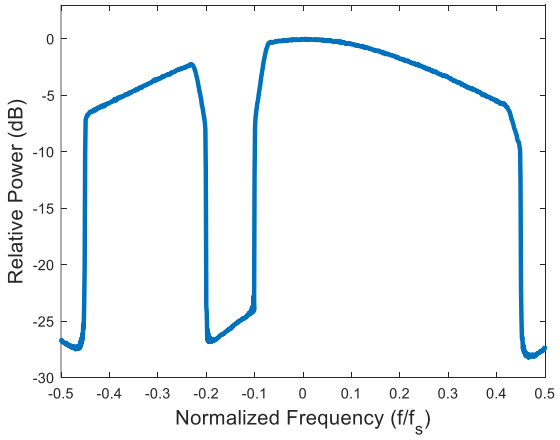

Fig. 1. Average spectral envelope for a set of notched waveforms

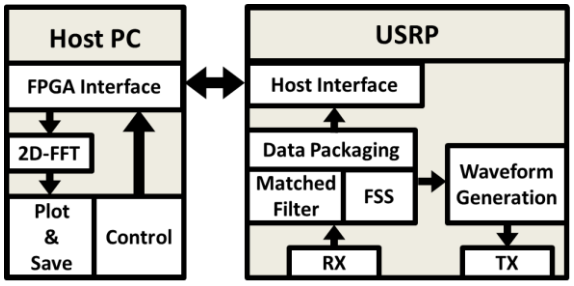

Fig. 2. Cognitive radar architecture on the SDRadar

The overall adaptation time T_{adapt} dictates how quickly the overall implementation can identify available spectrum and synthesize waveforms in reaction to environmental changes. It can be expressed as

$$\begin{aligned} T_{\text{adapt}} &= T_{\text{FSS}} + T_{\text{PRO}} + T_{\text{ZOROW}} \\ &= 120 + 28K + 28L \ \ \mu\text{s} \end{aligned} \tag{9}$$

where the lower line captures the currently achievable process times as implemented on the x310 FPGA, for K and L the respective number of iterations for PRO-FM and ZOROW. Here we use $K = 2$ and $L = 6$, which as shown in Fig. 1 can achieve 25 dB notch depths. Consequently, $T_{\text{adapt}} = 344$ μs.

In [15], a PRF of 2.22 kHz ($T_{\text{PRI}} = 550.6$ μs) was used. Software modification in the FPGA since then to operate the clock at twice the rate (from 100 to now 200 MHz), permits PRF values up to 4.4 kHz (so now $T_{\text{PRI}} = 225.3$ μs). Therefore, while the implementation in [15] incurred a 7-pulse latency (3.1 ms) at the lower PRF, the new instantiation could either update with no latency at the 2.22 kHz PRF or with a 1-pulse latency at the 4.44 kHz PRF.

Here we shall rely on the latter, meaning that as the rate of RFI hopping increases there will be a growing number of pulses in which the RFI and notch locations are mismatched (i.e. "collisions"). The reason for choosing this arrangement is because, in reality, there would be a degree of randomness that would almost certainly lead to some percentage of pulses with collisions.

If further latency is acceptable, based on an expectation of little/no RFI hopping, then deeper notches are also achievable via additional ZOROW iterations. Moreover, as SDR and RF-SoC technology progresses, these limits will become less restrictive.

IV. Evaluation of Real-Time Open-Air Operation

In [14] an open-air MTI test was performed based on prior observation and determination of notched waveforms, i.e. not reacting in real-time. Here we basically repeat that test but use the SDRadar, along with the procedure outlined above, to generate new notched waveforms in real-time as the RFI moves around in frequency. As before, this open-air test took place on the roof of Nichols Hall on the University of Kansas campus, observing the intersection of 23rd and Iowa streets roughly 1.1 km away. Fig. 3 provides a block diagram of test setup components, while Figs. 4 and 5 respectively show photos of the SDRadar (using separate transmit/receive antennas) and the location of the nearby RFI source.

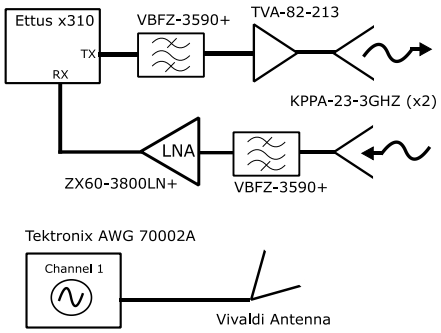

Fig. 3. Test setup overview, with sense-and-notch radar (top) and dynamic interferer (bottom)

Fig. 4. Open-air test setup: Ettus x310 SDRadar (white oval) and illuminated traffic intersection (green oval)

Fig. 5. Open-air test setup: interference source (red oval)

The SDRadar operates at 3.5 GHz and measures complex baseband data after receive down-conversion based on a 100

MHz sample clock. The pulse duration is 2.56 μs, which corresponds to a duty cycle of about 1.2 percent at the 4.44 kHz PRF. Each CPI comprises 1000 unique pulsed waveforms.

The RFI source is produced by a Tektronix AWG connected to a quad-ridge horn antenna, which transmits a single contiguous signal comprised of OFDM subcarriers having a 10 MHz bandwidth that randomly hops in frequency over the operating band at time intervals of T_{RFI}, which corresponds to a hopping rate of $f_{\mathrm{RFI}} = 1/T_{\mathrm{RFI}}$. In addition to a stationary RFI case, we consider $T_{\mathrm{RFI}} = 50$ ms, 10 ms, and 0.6 ms, which correspond to $f_{\mathrm{RFI}} = 20$ Hz, 100 Hz, and 1.66 kHz. A full-band RFM waveform case with no interference present is included for comparison. For $T_{\mathrm{PRI}} = 225.3$ μs, these cases amount to hopping of roughly 5, 23, and 375 times during the CPI (the RFI and SDRadar are not synchronized so the precise number could vary). Here we only consider a single hopping RFI source, though no change is needed to realize an arbitrary number of RFI sources/notches. Of course, further degradation is expected due to less available bandwidth for the radar to operate. Moreover, because the focus here was on demonstrating real-time notched waveform design/generation, clutter cancellation has not yet been incorporated.

To establish a baseline case, Fig. 6 illustrates the range/Doppler response for a CPI of full-band PRO-FM waveforms when no interference is present. Within the red ovals, we can discern movers that are detectable against the background. However, once the RFI is turned on (Fig. 7), the movers are no longer visible. When sense-and-notch operation is engaged for this stationary RFI case, movers once again become visible (Fig. 8). While arguably not necessary in this case, each notched waveform in the CPI is produced according to real-time sensing of RFI on a per-pulse basis. Comparison of the background responses in Figs. 6 and 8 shows an increase of a few dB for the latter, which is due to notch depth being limited to 25 dB here as a trade-off for real-time responsiveness.

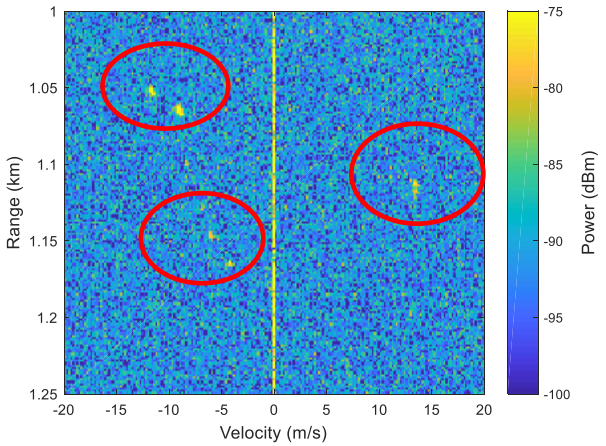

Fig. 6. Simple SDRadar, full-band PRO-FM, without RFI

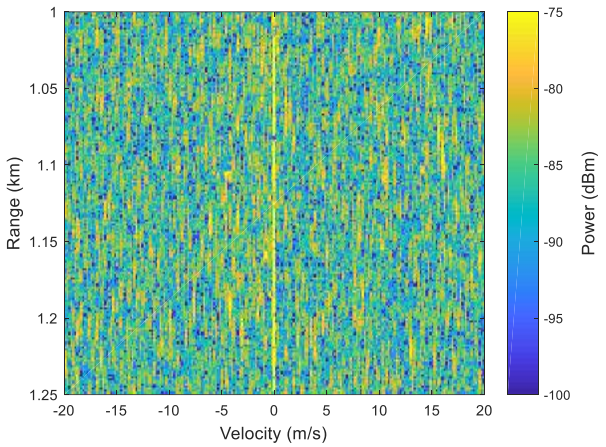

Fig. 7. Simple SDRadar, full-band PRO-FM, with stationary RFI

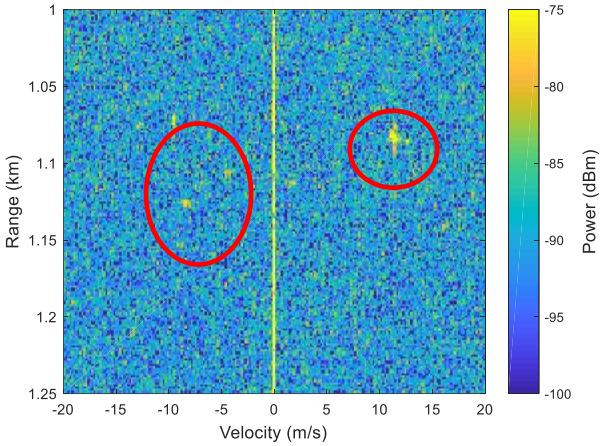

Fig. 8. Sense-and-notch SDRadar, with stationary RFI

We now allow the RFI to change dynamically at different rates, as illustrated in Figs. 9-11. It is observed that hopping every 50 ms in Fig. 9 is qualitatively the same as Fig. 8 because the RFI hopping rate is slow enough that additional clutter modulation induced by dynamic notching remains below the background response from RFI leakage.

As the hopping rate increases to occurring every 10 ms in Fig. 10, clutter modulation begins to arise (see dashed red oval) that can mask movers if not properly compensated, which is not incorporated here but has been investigated and experimentally demonstrated in [21-24]. However, we can still see movers present within the solid red circles.

Finally, when the hopping increases again to changing every 0.6 ms, Fig. 11 shows that clutter modulation has now grown to mask the movers. Moreover, with the PRI interval of 225.3 μs relative to the RFI hopping every 600 μs, the number of latency-induced collisions grows significant. In short, there is a need for further reduction of T_{adapt} if RFI becomes more dynamic.

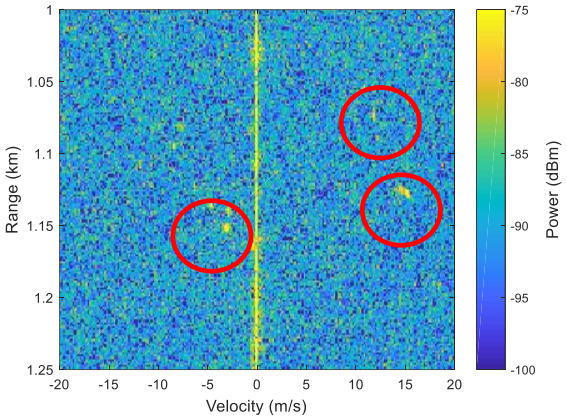

Fig. 9. Sense-and-notch SDRadar, RFI hopping every 50 ms

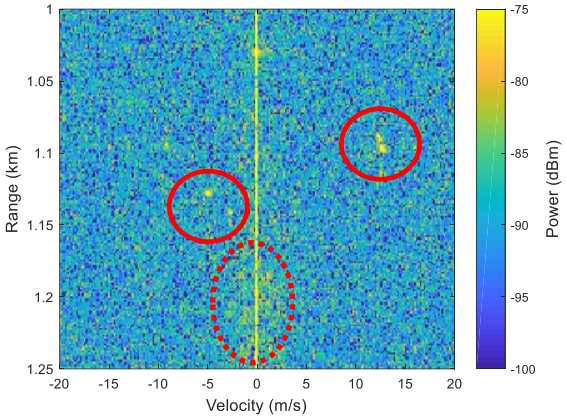

Fig. 10. Sense-and-notch SDRadar, RFI hopping every 10 ms

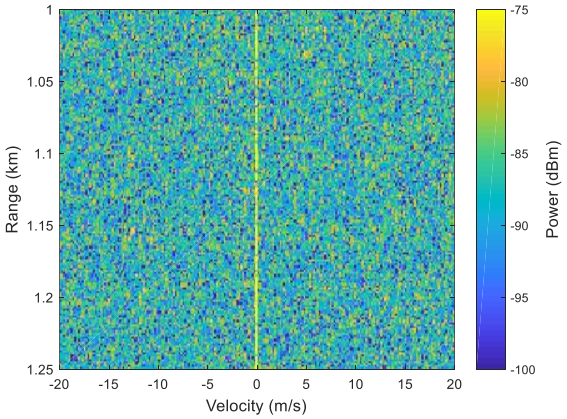

Fig. 11. Sense-and-notch SDRadar, RFI hopping every 0.6 ms

V. Conclusions

A real-time open-air experimental demonstration of a cognitive sense-and-notch radar capability has been shown to have practical feasibility. This approach addresses the limiting factors of physical generation of on-the-fly notched waveform design, hardware fidelity effects, and acceptable latency for response time. Of course, the increasing complexity of the RF environment, including a multiplicity of distributed and dynamic spectrum users, will continue to drive the need for faster responses of higher quality (in this context, deeper) notches. As required adaptation rates are driven faster by greater congestion, techniques to mitigate clutter modulation effects also become critical.

References

[1] H. Griffiths, et al., "Radar spectrum engineering and management: technical and regulatory issues," *Proc. IEEE*, vol. 103, no. 1, pp. 85-102, Jan. 2015.

[2] A. F. Martone *et al*., "Closing the Loop on Cognitive Radar for Spectrum Sharing," *IEEE Aerospace and Electronic Systems Magazine*, vol. 36, no. 9, pp. 44-55, 1 Sept. 2021

[3] A. Martone, M. Amin, "A view on radar and communication systems coexistence and dual functionality in the era of spectrum sensing," *Digital Signal Processing*, 2021

[4] S.D. Blunt, E.S. Perrins, *Radar & Communication Spectrum Sharing*, SciTech Publishing, 2018.

[5] G. Fabrizio, *High Frequency Over-the-Horizon Radar: Fundamental Principles, Signal Processing, and Practical Applications*, McGraw-Hill, 2013.

[6] M. Davis, *Foliage Penetration Radar – Detection and Characterization of Objects Under Trees*, SciTech Publishing, 2011.

[7] M.J. Lindenfeld, "Sparse frequency transmit-and-receive waveform design," *IEEE Trans. Aerospace & Electronic Systems*, vol. 40, no. 3, pp. 851-861, July 2004.

[8] K. Gerlach, M.R. Frey, M.J. Steiner, A. Shackelford, "Spectral nulling on transmit via nonlinear FM radar waveforms," *IEEE Trans. Aerospace & Electronic Systems*, vol. 47, no. 2, pp. 1507-1515, Apr. 2011.

[9] C. Nunn, L.R. Moyer, "Spectrally-compliant waveforms for wideband radar," *IEEE Aerospace & Electronic Systems Mag*., vol. 27, no. 8, pp. 11-15, Aug. 2012.

[10] L.K. Patton, B.D. Rigling, "Phase retrieval for radar waveform optimization," *IEEE Trans. Aerospace & Electronic Systems*, vol. 48, no. 4, pp. 3287-3302, Oct. 2012.

[11] T. Higgins, T. Webster, A.K. Shackelford, "Mitigating interference via spatial and spectral nulling," *IET Radar, Sonar & Navigation*, vol. 8, no. 2, pp. 84-93, Feb. 2014.

[12] A. Aubry, A. De Maio, M.A. Govoni, L. Martino, "On the design of multi-spectrally constrained constant modulus radar signals," *IEEE Trans. Signal Processing*, vol. 68, pp. 2231-2243, Apr. 2020

[13] A. Martone, K. Ranney, K. Sherbondy, K. Gallagher, S. Blunt, "Spectrum allocation for non-cooperative radar coexistence," *IEEE Trans. Aerospace & Electronic Systems*, vol. 54, no. 1, pp. 90-105, Feb. 2018.

[14] B. Ravenscroft, J.W. Owen, J. Jakabosky, S.D. Blunt, A.F. Martone, K.D. Sherbondy, "Experimental demonstration and analysis of cognitive spectrum sensing and notching for radar," *IET Radar, Sonar & Navigation*, vol. 12, no. 12, pp. 1466-1475, Dec. 2018.

[15] J.W. Owen, C.A. Mohr, B.H. Kirk, S.D. Blunt, A.F. Martone, K.D. Sherbondy, "Demonstration of real-time cognitive radar using spectrally-notched random FM waveforms," *IEEE Intl. Radar Conf.*, Washington, DC, Apr. 2020.

[16] S.D. Blunt, et al., "Principles & applications of random FM radar waveform design," *IEEE Aerospace & Electronic Systems Mag*., vol. 35, no. 10, pp. 20-28, Oct. 2020.

[17] C.A. Mohr, J.W. Owen, S.D. Blunt, C.T. Allen, "Zero-order reconstruction optimization of waveforms (ZOROW) for modest DAC rates," *IEEE Intl. Radar Conf.*, Washington, DC, Apr. 2020.

[18] A. Aubry, V. Carotenuto, A. De Maio, A. Farina, A. Izzo, R.S. Lo Moriello, "Assessing power amplifier impairments and digital pre-distortion on radar waveforms for spectral coexistence," to appear in *IEEE Trans. Aerospace & Electronic Systems*.

[19] C.A. Mohr, S.D. Blunt, "Analytical spectrum representation for physical waveform optimization requiring extreme fidelity," *IEEE Radar Conf.*, Boston, MA, Apr. 2019.

[20] J. Jakabosky, S.D. Blunt, B. Himed, "Spectral-shape optimized FM noise radar for pulse agility," *IEEE Radar Conf.*, Philadelphia, PA, May 2016.

[21] J. Owen, B. Ravenscroft, S.D. Blunt, “Devoid clutter capture and filling (DeCCaF) to compensate for intra-CPI spectral notch variation,” *Intl. Radar Conf.*, Toulon, France, Sept. 2019.

[22] B.H. Kirk, A.F. Martone, K.D. Sherbondy, R.M. Narayanan, “Mitigation of target distortion in pulse-agile sensors via Richardson-Lucy deconvolution,” *Electronics Letters*, vol. 55, no. 23, pp. 1249-1252, Nov. 2019.

[23] B. Ravenscroft, J.W. Owen, B.H. Kirk, S.D. Blunt, A.F. Martone, K.D. Sherbondy, R.M. Narayanan, “Experimental assessment of joint range-doppler processing to address clutter modulation from dynamic radar spectrum sharing," *IEEE Intl. Radar Conf.*, Washington, DC, Apr. 2020.

[24] C. Jones, B. Ravenscroft, J. Vogel, S.M. Shontz, T. Higgins, K. Wagner, S. Blunt, “Computationally efficient joint-domain clutter cancellation for waveform-agile radar,” *IEEE Radar Conf.*, Atlanta, GA, May 2021.